Two-gap superconductivity in ZrB_{12}: Temperature dependence of critical magnetic fields in single crystals

V. A. Gasparov, N. S. Sidorov, and I. I. Zver'kova
Institute of Solid State Physics RAS, 142432 Chernogolovka, Moscow District, Russia
(Received 26 August 2005; revised manuscript received 30 December 2005; published 21 March 2006)

We report the measurements of the temperature dependence of the resistivity, $\rho(T)$, magnetic penetration depth, $\lambda(T)$, the lower, $H_{c1}(T)$, and upper, $H_{c2}(T)$, critical magnetic fields, for single crystals of dodecaboride ZrB_{12}, diboride ZrB_2, and thin films of diboride MgB_2. We observe a number of deviations from conventional behavior in these materials. Although ZrB_{12} behaves like a simple metal in the normal state, the resistive Debye temperature, 300 K, is three times smaller relative to that (800–1200 K) calculated from the specific heat, $C(T)$, data. We observe predominantly quadratic temperature behavior of resistivity in ZrB_{12} below 25 K and in ZrB_2 below 100 K, indicating the possible importance of the electron-electron interaction in these borides. Superfluid density of ZrB_{12} displays unconventional temperature dependence with pronounced shoulder at T/T_c equal to 0.65. Contrary to conventional theories we found a linear temperature dependence of $H_{c2}(T)$ for ZrB_{12} from T_c down to 0.35 K. We suggest that both $\lambda(T)$ and $H_{c2}(T)$ dependencies in ZrB_{12} can be explained by a two band BCS model with different superconducting gap and T_c.

DOI: 10.1103/PhysRevB.73.094510 PACS number(s): 74.70.Ad, 74.25.Nf, 72.15.Gd, 74.25.Ha

I. INTRODUCTION

The recent discovery of superconductivity in magnesium diboride[1] has initiated a substantial interest in potential high temperature superconducting transition in other borides.[2] Yet, only nonstoichiometric boride compounds ($MoB_{2.5}$, $NbB_{2.5}$, Mo_2B, W_2B, $BeB_{2.75}$) demonstrate such transition.[3–6] The absence of superconducting transition in stoichiometric borides is clearly not in line with the old idea about superconductivity in metallic hydrogen[7] recently applied by Kortus *et al.*[8] to explain superconductivity in MgB_2. A potential clue to this contradiction my lay not in the small mass of the boron atoms but rather in crystal structure of these boron compounds, in particular in their cluster structure. Crystal structure clearly plays an important role in superconductivity. Although it is widely accepted that the layered structure is crucial for high-T_c superconductivity, one can argue that clusters of light atoms are important for high-T_c as well. In particular, there are a number of rather high-T_c superconductors among three-dimensional (3D) cluster compounds. Those are alkali metal doped C_{60} compounds (fullerides) Me_3C_{60} (Me=K, Na, Rb, Cs) with the highest T_c up to 33 K for $RbCs_2C_{60}$.[9,10] It is also known that boron atoms form clusters. These are octahedral B_6 clusters in MeB_6, icosahedral B_{12} clusters in β-rhombohedral boron, and cubo-octahedral B_{12} clusters in MeB_{12}.

The quest for superconductivity in these cluster compounds has a long history. Several superconducting cubic hexaborides, MeB_6, and dodecaborides, MeB_{12}, have been discovered by Matthias *et al.* back in late 1960's[11] (Me=Sc, Y, Zr, La, Lu, Th). Many other cluster borides (Me=Ce, Pr, Nd, Eu, Gd, Tb, Dy, Ho, Er, Tm) were found to be ferromagnetic or antiferromagnetic.[11,12] It was suggested[3] that the superconductivity in YB_6 and ZrB_{12} (T_c of 6.5–7.1 and 6.03 K, respectively[3]) is exactly due to the effect of a cluster of light boron atoms. At the same time, a much smaller isotope effect on T_c for boron in comparison with Zr isotopic substitution suggests that the boron in ZrB_{12} serves as inert background for the Zr-driven superconductivity.[13,14] Clearly a systematic study of ZrB_{12} is needed to address the question of superconductivity in this compound.

Superconductivity in ZrB_{12}-based compounds was discovered a while ago,[11] however, there has been little and controversial effort devoted to the study of basic superconducting and the electron transport properties of these compounds. In our recent study of the electron transport and superconducting properties of polycrystalline ZrB_{12},[15–18] we demonstrated that this compound behaves like a normal metal with the usual Bloch-Grüneisen dependence of $\rho(T)$ but with rather low resistive Debye temperature (T_R=280 K). The latter is almost three times smaller than Debye temperature obtained from specific heat $C(T)$ data.[19] We observed linear temperature dependence of $\lambda(T)$ below $T_c/2$ which could be evidence of d-wave pairing in this compound. Furthermore, contrary to conventional theories, we found a linear temperature dependence of $H_{c2}(T)$. Recently the band structure calculations of ZrB_{12} (Ref. 20) have been also reported. It was concluded that the band structure of ZrB_{12} is composed of one open and two closed Fermi surface sheets.

Our data contradict the report of Daghero *et al.*[21] dealing with the point-contact spectroscopy (PCS) of single crystals of ZrB_{12} at temperatures close to T_c. In Daghero's report it was concluded that ZrB_{12} is a strong coupling s-wave superconductor, with $2\Delta(0)/k_BT_c$=4.7. Tsindlekht *et al.*[22] came to a similar conclusion from tunneling and magnetic characterization of ZrB_{12} single crystals at the temperatures also very close to T_c (4.5–6 K). Lortz *et al.*[19] and Wang *et al.*[23] reported $C(T)$, $\rho(T)$, magnetic susceptibility, and thermal expansion measurements of ZrB_{12} samples prepared by one of us (V.A.G.) and concluded that it is a single gap marginal BCS superconductor which undergoes transition from a type-I superconductor near T_c to a type-II superconductor below 4.6 K with $2\Delta(0)/k_BT_c$=3.7, the value that is lower

 ©2006 The American Physical Society

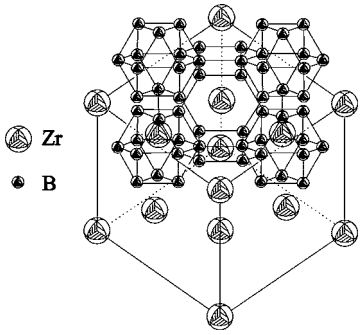

FIG. 1. Lattice structure of dodecaboride ZrB_{12}. For clarity B_{12} clusters are shown only on the upper face of the lattice.

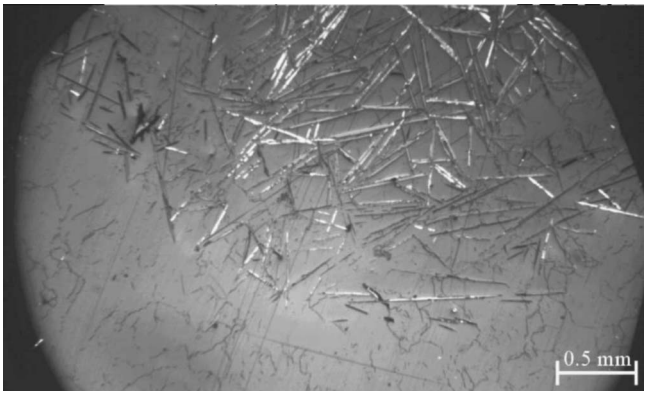

FIG. 2. Etching pattern of a ZrB_{12} single crystal cross section in the (100) plane from the same parts of ingot as in Refs. 19 and 21–23. The needlelike long grains are ZrB_2 phase, while the small black lines correspond to etching pits from small angle boundaries.

than that obtained from PCS (4.7)[21] and scanning tunneling microscopy data.[22] A large difference in H_{c2} characteristics reported in the above-mentioned papers was discussed in terms of surface superconductivity. Most of the features of MgB_2 discovered so far can be explained by a two band superconductivity model.[24] We believe that a test of the predictions of this model for ZrB_{12} may explain observed controversy of published data. Knowledge of the electron transport and superconducting properties in this cluster compound is crucial for understanding these conflicting results.

This has been the motivation for current systematic study of the temperature dependencies of $\rho(T)$, $\lambda(T)$, lower $H_{c1}(T)$, and upper $H_{c2}(T)$, critical magnetic fields in single crystals of ZrB_{12}. In this paper, we confirm unusual superconducting properties of ZrB_{12} observed in Refs. 15–18 and argue that the published results can be reconciled by two-band superconductivity. Comparative data from ZrB_2 single crystals and thin films of MgB_2 are also presented.

The structure of this paper is as follows. In Sec. II we report on the samples details and experimental techniques. Section III describes the electron transport in these compounds and Sec. IV describes the temperature dependence of $\lambda(T)$ in ZrB_{12} samples and MgB_2 thin films. The data on $H_{c1}(T)$ and $H_{c2}(T)$ are presented in Sec. V. Section VI contains our conclusions.

II. EXPERIMENTAL SETUP

Under ambient conditions, dodecaboride ZrB_{12} crystallizes in the fcc structure of the UB_{12} type (space group $Fm3m$, $a=0.74075$ nm,[25,26] see Fig. 1). In this structure, the Zr atoms are located at interstitial openings among the close-packed B_{12} clusters. In contrast, ZrB_2 shows a phase consisting of a two-dimensional graphitelike monolayer of boron atoms with a honeycomb lattice structure and the lattice parameters $a=0.30815$ nm and $c=0.35191$ nm (space group $P6/mmm$), intercalated with a Zr monolayer.[2]

Our ZrB_{12} and ZrB_2 single crystals were grown using a floating-zone method[17,18,25] similar to Ref. 26. The obtained single crystal ingots had a typical diameter of about 5 to 6 mm and a length of 40 mm. Measured specific weight of the ZrB_{12} rod was 3.60 g/cm^3, in a good agreement with the theoretical density. The cell parameter of ZrB_{12}, $a=0.74072\pm0.00005$ nm, is very close to the published values.[26] To assure good quality of our samples we performed the metallographic and x-ray investigations of as-grown ingots. We discovered that most parts of the ZrB_{12} ingot contained a needlelike phase of nonsuperconducting ZrB_2 (see Fig. 2). We believe that ZrB_2 needles are due to preparation of ZrB_{12} single crystals from a mixture of a certain amount of ZrB_2 and an excess of boron.[18,25] Therefore special care has been taken to cut the samples from ZrB_2 phase-free parts.

For this study, two highly crystalline, superconducting films of MgB_2 were grown on an *r*-plane sapphire substrate in a two-step process.[27] Deposition of boron precursor films via electron-beam evaporation was followed by *ex situ* post-annealing at 890 °C in the presence of bulk MgB_2 and Mg vapor. We investigated films of 500 and 700 nm thickness, with corresponding T_{c0}'s of 38 and 39.2 K, respectively. The details of the preparation technique are described elsewhere.[27]

We used the spark erosion technique to cut the single crystal ingots into rectangular ⟨100⟩ oriented bars of about $0.5\times0.5\times8$ mm^3. The samples were lapped with diamond paste and etched in boiled nitrogen acid to remove any damage induced by lapping deteriorated surface layers. A standard four-probe ac (9 Hz) technique was used for resistance measurements. We used *Epotek H20E* silver epoxy for electrical contacts. Because the sample has a shape of a long rectangular bar its demagnetization factor is nearly zero. A well-defined geometry of the samples provided for the precise $\rho(T)$ and superconducting properties measurements. Temperature was measured with platinum (PT-103) and carbon glass (CGR-1-500) sensors. The measurements were performed in the liquid helium variable temperature cryostat in the temperature range between 1.3 and 350 K. Magnetic measurements of $\rho(T,H)$ and $\lambda(T,H)$ were carried out using a superconducting coil in applied fields of up to 6 T down to 1.3 K. Additional dc and ac $\rho(H)$ measurements were performed in the National High Magnetic Field Laboratory in Tallahassee, Florida (NHMFL) at temperatures down to 0.35 K. The dc magnetic field was applied in the direction of the current flow. The critical temperature of the ZrB_{12} samples, measured by ac susceptibility and $\rho(T)$, was found to be $T_{c0}=6.0$ K.

We used the radio frequency *LC* technique[28] to measure $\lambda(T)$ of ZrB_{12} samples. This technique employs a rectangular solenoid coil into which the sample is placed. The coil is a part of the *LC* circuit driven by a marginal oscillator operating at 2–10 MHz, or by the impedance meter (VM-508 TESLA 2–50 MHz). Changes in $\lambda(T)$ of the sample lead to the change of the coil's inductance that in turn results in the change of the resonance frequency of the *LC* circuit. The connection between parameters of the circuit and $\lambda(T)$ is described by following equation:

$$\lambda(T) - \lambda(0) = \delta \frac{f^{-2}(T) - f^{-2}(0)}{f^{-2}(T_c) - f^{-2}(0)}. \quad (1)$$

Here $\delta = 0.5(c^2\rho/2\pi\omega)^{1/2}$ is the imaginary part of the skin depth above T_c,[29] which was determined from the $\rho(T)$ measurements close to T_c, $f(T)$ is the resonance frequency of the circuit at arbitrary temperature T, and $f(T_c)$ and $f(0)$ are the resonance frequency of the circuit at the superconducting transition and at zero temperature, respectively.

The $\lambda(T)$ dependence in thin MgB_2 films was investigated employing a single coil mutual inductance technique. This technique, originally proposed in Ref. 30 and improved in Ref. 31, takes advantage of the well-known two-coil geometry. It was successfully used for the observation of the Berezinskii-Kosterlitz-Thouless vortex-antivortex unbinding transition in ultrathin $YBa_2Cu_3O_{7-x}$ films[32] as well as for study of the $\lambda(T)$ dependence on MgB_2 films.[33] In this radio-frequency technique one measures the temperature dependence of the complex impedance of the *LC* circuit formed with a one-layer pancake coil located in the proximity ($\approx$0.1 mm) of the film. Both sample and coil are in a vacuum, but the coil holder is thermally connected with helium bath, while the sample holder is isolated and may be heated. During the experiment the coil was kept at 2.5 K, whereas the sample temperature has been varied from 2.5 up to 100 K. Such design allows us to eliminate possible effects in temperature changes in *L* and *C* on the measurements.

The complex mutual inductance *M* between the coil and the film can be obtained through

$$\mathrm{Re}\, M(T) = L_0\left(\frac{f_0^2}{f^2(T)} - 1\right), \quad (2)$$

$$\mathrm{Im}\, M(T) = \frac{1}{[2\pi f(T)]^3 C^2}\left[\frac{1}{Z(T)} - \frac{1}{Z_0(T)} \cdot \frac{f^2(T)}{f_0^2}\right]. \quad (3)$$

Here L, $Z(T)$, $f(T)$, L_0, $Z(0)$, and f_0 are the inductance, the real part of impedance, and the resonant frequency of the circuit with and without the sample, respectively. In the London regime, where the high frequency losses are negligible, one can introduce $\Delta\,\mathrm{Re}\, M(T)$—the difference between temperature dependant real part of *M* of the coil with the sample, $\mathrm{Re}\, M(T)$, and that of the coil at T_0, $\mathrm{Re}\, M(T_0)$. This difference is a function of the London penetration depth $\lambda(T)$:

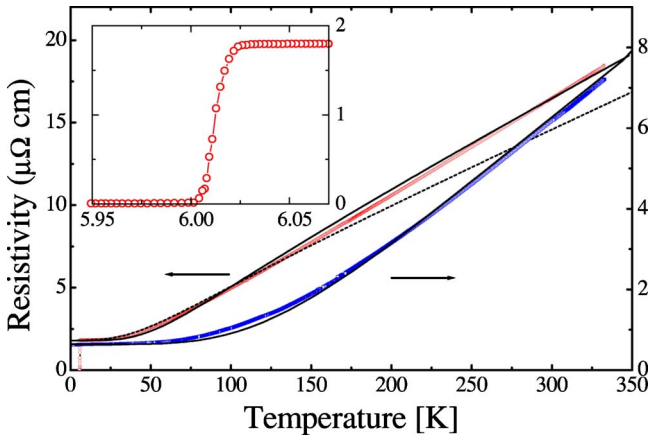

FIG. 3. (Color online) Temperature dependence of $\rho(T)$ for ZrB_{12} (circles) and ZrB_2 (squares) single crystal samples. The solid lines represent BG fits to the experimental data by Eq. (5). The dashed line is t^3 BG fit below 170 K with $T_R = 283$ K as in Ref. 21.

$$\Delta\,\mathrm{Re}\, M(T) = \pi\mu_0 \int_0^\infty \frac{M(q)dq}{1 + 2q\lambda\,\coth\left(\frac{d}{\lambda}\right)}, \quad (4)$$

where $M(q)$ plays the role of mutual inductance at a given wave number q in the film plane and depends on the sample-coil distance, d is the sample thickness (additional details can be found in Ref. 31). A change in $\Delta\,\mathrm{Re}\, M(T)$ is detected as a change of resonant frequency $f(T)$ of the oscillating signal through Eq. (2). This change when put into Eq. (4) yields temperature dependent London penetration depth $\lambda(T)$. Thanks to Eq. (4), we can measure the $\lambda(T)$ of superconducting film by measuring the variation $\Delta\,\mathrm{Re}\, M(T)$ of coil impedance and convert them into $\lambda(T)$.

III. ELECTRON TRANSPORT

Figure 3 shows the temperature dependence of $\rho(T)$ of ZrB_{12} and ZrB_2 single crystal samples. To emphasize the variation of $\rho(T)$ in a superconductive state, we plot these data in the inset. The transition temperature ($T_{c0} = 6.0$ K) is consistent with the previously reported values for ZrB_{12} (6.03 K)[11,13] and is larger than that of ZrB_2 polycrystalline samples (5.5 K).[2] The ZrB_{12} samples demonstrate a remarkably narrow transition with $\Delta T = 0.04$ K. We believe that such a narrow transition is an indicator of the good quality of our samples.

Figure 3 does not show any hints of the superconducting transition in ZrB_2 single crystals down to 1.3 K,[18] even though superconductivity was observed before at 5.5 K in polycrystalline samples.[2] It was recently suggested[34] that this apparent contradiction could be associated with nonstoichiometry in the zirconium sublattice. Based on the electron structure calculation it was suggested that the Fermi level in ZrB_2 is located in the pseudogap.[34] The presence of Zr defects in $Zr_{0.75}B_2$ leads to the appearance of a very intense peak in the density of states in the vicinity of the pseudogap and subsequent superconductivity. We strongly believe that

observation of superconductivity at 5.5 K in polycrystalline samples of ZrB_2 was due to nonstoichiometry of our samples. It is likely that recent observations of superconductivity in nonstoichiometric $Nb_{1-x}B_2$ compounds[4,5] as well as in other nonstoichiometric borides[3,6] have the same origin.

As we can see from Fig. 3, despite the fact that ZrB_{12} contains mostly boron, its room temperature $\rho(T)$ is only twice as large as that of single crystal samples of ZrB_2. The $\rho(T)$ of ZrB_{12} is linear above 90 K with the slope markedly steeper than in ZrB_2, with rather low residual resistivity ratio $\rho_{300\ K}/\rho_{6\ K} \approx 10$. One can predict a nearly isotropic $\rho(T)$ dependence for fcc ZrB_{12}, which can be described by the Bloch-Grüneisen (BG) equation of the electron-phonon (e-p) scattering rate:[35]

$$\rho(t) - \rho(0) = 4\rho_1 t^5 \int_0^{1/t} \frac{x^5 e^x dx}{(e^x - 1)^2} = 4\rho_1 t^5 J_5(1/t). \quad (5)$$

Here, $\rho(0)$ is the residual resistivity, $\rho_1 = d\rho(T)/dt$ is the slope of $\rho(T)$ at high $T > T_R$, $t = T/T_R$, T_R is the resistive Debye temperature, and $J_5(1/t)$ is the Debye integral.

It is clear from Fig. 3 that the BG model nicely describes the $\rho(T)$ dependence of both borides, indicating the importance of e-p interaction. It is remarkable that this description works well with constant $T_R = 300$ K, which is very close to $T_R = 280$ K observed on polycrystalline samples.[16] Clearly, ZrB_2 ($T_R = 700$ K) and ZrB_{12} have very different $\rho(T)$ dependence due to different T_R. At the same time the phonon Debye temperature, T_D, for ZrB_{12} calculated from $C(T)$ on rather large samples ($4.7 \times 4.8 \times 2.9$ mm^3) prepared by one of us (V.A.G.) (without metallographic study),[19,23] is three times higher. Furthermore, T_D increases from 800 to 1200 K as temperature rises from T_c up to room temperature. We believe that this inconsistency of T_R and T_D can be explained by limitation of T_R by a cutoff phonon wave vector $q = k_B T/\hbar s$. The latter is limited by the Fermi surface (FS) diameter $2k_F$ (Ref. 36) rather than the highest phonon frequency in the phonon spectrum.[18] Besides some problems may arise in Refs. 19 and 23 due to use of ZrB_2 phase rich samples as in Fig. 2 (see below).

Actually, $\rho(T)$ of ZrB_{12} and ZrB_2, samples deviates from the BG model at low temperatures.[18] We have reported for ZrB_{12}, ZrB_2, and MgB_2 that such deviation is consistent with a sum of electron-electron (e-e), aT^2, and e-p, bT^5, contributions to the low-T $\rho(T)$ data. The coefficient $b = 497.6\rho_1/T_R^5$ in this plot gives another measure of T_R from low-T $\rho(T)$ data. We found this T_R in a good agreement with that extracted from full-T BG fit for both ZrB_2 and ZrB_{12} samples. Therefore the data extracted from this two-term fit are self-consistent with the full Eq. (5) fit. We would like to stress that this observation is only possible in the approximation of constant T_R, which is in contradiction with specific heat data.[19] Notice also that the e-p contribution to resistivity $\rho(T)$ can be described through[37]

$$\rho_{ep}(T) \propto \int_0^{1/t} \alpha^2(k,\omega) F(\omega) \Phi(\varepsilon,\omega) d\omega, \quad (6)$$

where $\alpha^2(k,\omega)F(\omega)$ is the effective Eliashberg density of states of the phonons, that is e-p coupling function $\alpha^2(k,\omega)$ multiplied by the phonon density of states $F(\omega)$ with energy $\hbar\omega$.[37] The $\alpha^2(k,\omega)$ is proportional to the matrix element of e-p coupling averaged over phonon polarization, but only longitudinal phonons are responsible for e-p scattering for spherical FS. At the same time, the phonon specific heat, $C(T)$, can be expressed as

$$C_{ph} = 3R \int_0^{1/t} F(\omega)\Phi_1(\omega) d\omega. \quad (7)$$

Here $\Phi(\varepsilon,\omega)$ and $\Phi(\omega)$ are the occupation factors for e-p and phonon systems, respectively.[37] This means that different phonons are responsible for e-p $\rho(T)$ and $C(T)$. In particular, the transverse phonons are much less important for e-p scattering whereas both transverse and longitudinal phonons equally contribute to $C(T)$.

Borides have rather high T_D that depresses the e-p scattering, as a result the e-e scattering term may be much more pronounced. Indeed, we find very similar values of a-coefficient for ZrB_{12} and ZrB_2 samples in the basal plane ($a = 22$ and 15 pΩ cm K^{-2}, respectively).[18] It is interesting to note, however that these values are five times larger than the e-e term for transition metals [$a_{Mo} = 2.5$ pΩ cm K^{-2} and $a_W = 1.54$ pΩ cm K^{-2} (Ref. 18)]. In general, there are many scattering processes responsible for the T^2 term in $\rho(T)$ of metals. This term could be due to electron-impurity, electron-dislocation scattering, etc., induced deviation from Mattiessen rule. It is difficult to separate the contributions of these effects, thus it is presently not clear where exactly this T^2 term comes from.[18] Therefore additional experiments on more pure samples must be performed before a final conclusion about the origin of the T^2 term in borides can be drawn.

As we mentioned in the Introduction of this paper, there is a contradiction between our description of the $\rho(T)$ and that of Refs. 19 and 21. Daghero *et al.* suggested BG fit with t^3 dependence rather than t^5 on the similar single crystals at low $T < 170$ K.[21] The fit assumed model ω^2 dependence for the $\alpha^2(k,\omega)F(\omega)$ in Eq. (6). Such assumption yielded a good fit to their data at $T < 170$ K with the $T_R = 283$ K similar to our value of 300 K. We would like to stress, however, that there are strong objections to this modified t^3 BG model.[18] The main problem of this approach is that it completely ignores intrasheet small angle e-p scattering responsible for T^5 law and takes into account only intersheet scattering events. No evidence of this model was observed in transition and nontransition metals. To check the approach of Daghero's group we used it for our data. Figure 3 displays the BG fit with $\rho(T) - \rho(0) \propto t^3 J_3(1/t)$ in Eq. (5) at $T < 170$ K (dashed line). It is clear that this fit is far from consistency at higher T. We believe this is an indication that $\rho(T)$ cannot be fitted by a modified BG t^3 equation in the whole temperature range. We suggest that a sum of T^2 and T^5 contributions to the low-T $\rho(T)$ may be easily confused with a T^3 law.[18] Notice that our observation of BG T^5 intraband $\rho(T)$ dependence rather then intersheet T^3 law is very important for the given below two-T_c model of two-gap superconductivity for ZrB_{12}. In fact, this model is right in the limit of zero interband coupling. The two bands coupling converge two T_c to a single one.

Lortz *et al.*[19] report temperature dependence of $\rho(T)$ obtained on the samples cut from ones provided by our group. The $\rho(T)$ is nearly identical to our data, however, interpretation is different. Lorts *et al.* fitted $\rho(T)$ with the generalized Bloch-Grüneisen formula using a decomposition into Einstein modes of $\alpha^2(k,\omega)F(\omega)$. The same approach was applied to $C(T)$ data and it was concluded that there are similarities between $F(\omega)$ determined from $C(T)$ and $\alpha^2(k,\omega)F(\omega)$ from $\rho(T)$. However the fit to $\rho(T)$ data was obtained using six fitting parameters for $\alpha_k^2 F_k$ and $\rho(0)$. We believe such fit is not better than a simple Debye Eq. (5) fit with just two parameters: T_R and $\rho(0)$. Furthermore, it is not clear whether the Einstein model is applicable to ZrB_{12}. Finally, we note also that only phonons with a phonon wave vector $q=k_BT/\hbar s<2k_F$ can participate in $\rho(T)$.[36] Thus T_R is limited by the FS diameter $2k_F$ rather than the highest phonon frequency in the phonon spectrum, which in turn is important for T_D. Notice also that unconventional $T_D(T)$ dependence observed from $C(T)$ data in Refs. 19 and 23 may be due to the sample problems (see Fig. 2).

IV. PENETRATION DEPTH

In the BCS theory the London penetration depth is identical with $\lambda(T)$ for specular and diffuse surface scattering and for negligible nonlocal effects. For a BCS-type superconductor with the conventional *s*-wave pairing form, the $\lambda(T)$ has an exponentially vanishing temperature dependence below $T_c/2$ (where $\Delta(T)$ is almost constant):[38]

$$\lambda(T)=\lambda(0)\left[1+\sqrt{\frac{\pi\Delta(0)}{2k_BT}}\exp\left(-\frac{\Delta(0)}{k_BT}\right)\right] \tag{8}$$

for clean limit: $l>\xi$ and

$$\lambda(T)=\lambda(0)\sqrt{\frac{1}{\tanh\left(\frac{\Delta(0)}{2k_BT}\right)}} \tag{9}$$

for dirty limit: $l<\xi$.[39] Here $\Delta(0)$ is the energy gap and $\lambda(0)$ is the penetration depth at zero temperature. Close to T_c $\lambda(T)$ dependence has a BCS form:[29]

$$\lambda(T)=\frac{\lambda(0)}{\sqrt{2\left(1-\frac{T}{T_c}\right)}}. \tag{10}$$

Important problems for $\lambda(T)$ measurements are (i) determination of basic superconducting parameter $\lambda(0)$ and (ii) temperature dependence law, to see whether *s*-wave or *d*-wave pairing forms exist. Both these problems can be addressed from low-T $\lambda(T)$ dependence according to Eqs. (8) and (9). We used Eq. (1) to extrapolate the resonance frequency $f(T)$ of our *LC* circuit down to zero temperature. The inset to Fig. 4 shows $f^{-2}(T)\propto\lambda(T)-\lambda(0)$ used for determination $f(0)$. We would like to stress that one can use linear dependence of $f^{-2}(T)$ and hence $\lambda(T)-\lambda(0)$ below 3 K,[15–17] due to uncertainty with $f(0)$.

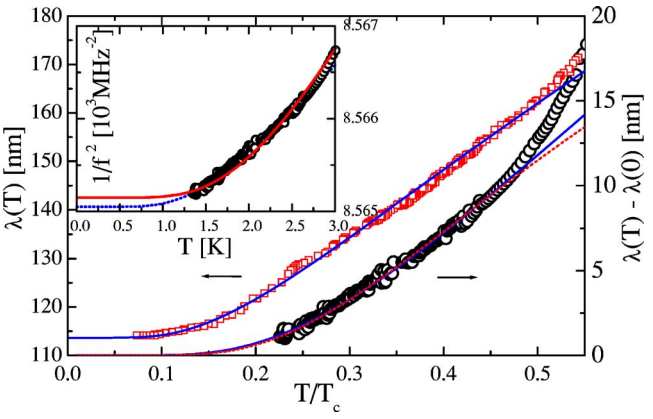

FIG. 4. (Color online) Temperature variation of the $\lambda(T)$ vs T/T_c for ZrB_{12} single crystal (circles) and MgB_2 thin film (squares) below $0.55T_c$. Solid curves represent the single gap dirty limit fit [Eq. (9)] and the dashed line represent the clean limit fit [Eq. (8)] for MgB_2 and ZrB_{12}. Inset shows $f^{-2}(T)$ and a result of fit by Eqs. (1) and (9).

The unconventional *d*-wave pairing symmetry causes the energy gap to be suppressed along nodal directions on the FS. This type of pairing should manifest itself through the linear temperature dependence of $\lambda(T)-\lambda(0)\propto T$ at low T. Such a linear T dependence of $\lambda(T)$ has been used as an fingerprint of *d*-wave pairing in cuprates.[40,41] At the same time the microwave $\lambda(T)$ data in fully oxygenated YBCO films show a picture which is consistent with the two-band *s*-wave superconductivity.[42] Recently, it was suggested[43] that a strictly linear T dependence of $\lambda(T)$ at low temperatures violates the third law of thermodynamics because it results in nonvanished entropy in the zero temperature limit. One can argue that a deviation of the linear T dependence of $\lambda(T)$ should be observed at low-T. Indeed, recent experiments on $\lambda(T)$ in cuprates indicate deviations from linearity at low-T from current carrying zero energy surface Andreev bound states.[44] We believe that the question about linear dependence of $\lambda(T)$ is still open therefore we use BCS Eqs. (8) and (9) to fit our data.

The dashed curve in the inset to Fig. 4 is a result of the fit by aid of BCS Eq. (9) for $\lambda(T)$ with $f(0)$ and $\Delta(0)$ as free parameters. Equation (1) defines the difference between extrapolated $\lambda(0)$ at zero temperature and that at the arbitrary temperature T, $\lambda(T)-\lambda(0)$. We would like to stress that $\lambda(T)-\lambda(0)$ data are robust relative to the change of the oscillator frequency. We observed no change in data when oscillator frequency has been increased from 2 to 10 MHz. Figure 4 shows how $\lambda(T)-\lambda(0)$ changes with reduced temperature, T/T_c, at low T for both MgB_2 (squares) and ZrB_{12} (circles). Our ZrB_{12} data do not extend to as low reduced temperatures as our data for MgB_2. This could lead to somewhat larger uncertainty in the estimates for the zero temperature resonance frequency $f(0)$, and hence $\lambda(0)=66$ nm and $\Delta(0)$ from low-T data for ZrB_{12}.

To address the problem with $\lambda(0)$ we plot $\lambda(T)-\lambda(0)$ data versus BCS reduced temperature: $1/\sqrt{2(1-T/T_c)}$ in the region close to T_c (see inset to Fig. 5). The advantage of this procedure is the insensitivity of such analysis to the choice

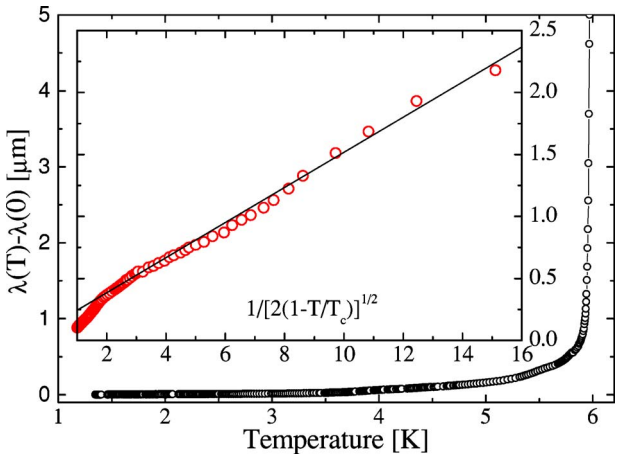

FIG. 5. (Color online) Temperature variations of $\lambda(T)$ for ZrB_{12} sample. The inset shows $\lambda(T)-\lambda(0)$ vs BCS reduced temperature.

of $f(0)$ on this temperature scale. The value of $T_c=5.992$ K used in this data analysis is obtained by getting best linear fit of the $\lambda(T)-\lambda(0)$ vs $[2(1-T/T_c)]^{-1/2}$ plot. Remarkably there is only a few millidegrees difference between T_c obtained from the fit and actual T_{c0}. We use the slope of $\lambda(T)-\lambda(0)$ vs $1/\sqrt{2(1-T/T_c)}$ and Eq. (10) to obtain the value of $\lambda(0)=143$ nm. To assure that this $\lambda(0)$ is in agreement with low-T data, we fit the f^{-2} vs T data with Eqs. (1) and (9) using fixed $\lambda(0)=143$ nm and free $\Delta(0)$ at low T. This fit is shown in the inset to Fig. 4 by the solid curve. It is clear from this inset that high-T $\lambda(0)$ is in agreement with low-T experimental data.

After completion of the analysis of the residual penetration depth we attempt to estimate the residual mean free path l. In particular we employ Drude formula $[\rho(0)=3/N_0 l v_F e^2]$ where we use measured $\rho(0)=1.8\ \mu\Omega$ cm, the electron density of states determined from $C(T)$ data, $N_0=1.83\times10^{22}$ st/eV cm,[3,23] and the electron Fermi velocity of $v_F=1.9\times10^8$ cm/s [determined from $E(k)$ data[20]], to obtain $l=33$ nm. This value is smaller than a coherence length [$\xi(0)=45$ nm, see below] indicating that our samples are in dirty limit. This is confirmed in Fig. 4 by slightly better fits of the $\lambda(T)-\lambda(0)$ with Eq. (9) up to $T/T_c=0.5$ (solid curve) relative to the clean limit [Eq. (8)] (dashed curve). In order to investigate the temperature dependence of $\lambda(T)$ in the whole temperature region, in Fig. 6 we plot the superfluid density $\lambda^2(0)\lambda^2(T)$ versus the reduced T/T_c for the ZrB_{12} sample using the $\lambda(0)=143$ nm determined from one gap fit close to T_c [Eq. (10)] and $\lambda(0)=66$ nm as determined from low-T fit [Eq. (9)], for comparison.

One can easily notice from Fig. 6 an unconventional behavior of ZrB_{12} superfluid density with pronounced shoulder at T/T_c equal to 0.65 for both $\lambda(0)$. This feature can be explained by a model of two independent BCS superconducting bands with different plasma frequencies, gaps, and T_c's.[24] We label these two bands as p- and d-bands according to electron structure of ZrB_{12}.[20] Assuming parallel currents through alternating subsystems, the conductivity is a sum of partial bands conductivities. The imaginary part of the conductivity is proportional to $1/\lambda^2$, thus we can write in dirty limit:[45]

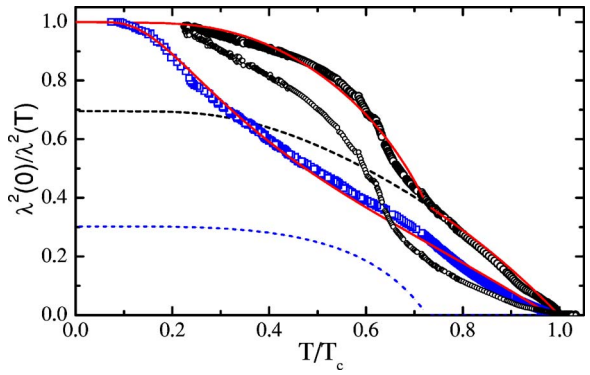

FIG. 6. (Color online) Superfluid density, $[\lambda(0)/\lambda(T)]^2$, of the ZrB_{12} sample for the $\lambda(0)=143$ nm (open circles), $\lambda(0)=66$ nm (small circles), and MgB_2 thin film (squares). The predicted behavior of $[\lambda(0)/\lambda(T)]^2$ within the two band model as described in the text is shown by the solid, dashed (p-band), and dotted (d-band) lines. The solid line represents single band BCS fit of MgB_2 data using $2\Delta(0)/k_BT_c$ as fit parameter.

$$\frac{1}{\lambda^2(T)}=\frac{\Delta_p(T)\tanh\left(\frac{\Delta_p}{2k_BT}\right)}{\lambda_p^2(0)\Delta_p(0)}+\frac{\Delta_d(T)\tanh\left(\frac{\Delta_d}{2k_BT}\right)}{\lambda_d^2(0)\Delta_d(0)}. \quad (11)$$

Here Δ_i is the superconducting energy gap and $\lambda_i(0)$ is residual penetration depth in the p- or d-band. Using this two gap $\lambda(T)$ BCS-like dependence and interpolation formula $\Delta(T)=\Delta(0)\tanh(1.88\sqrt{T_c/T-1})$ we fit the experimental data with six fitting parameters: λ_i, Δ_i, and T_c^i. From this fit we obtain $T_c^p=6.0$ K, $T_c^d=4.35$ K, $\Delta_p(0)=0.73$ meV, $\Delta_d(0)=2.1$ meV, $\lambda_p(0)=172$ nm, and $\lambda_d(0)=260$ nm, for p- and d-bands, respectively. Dashed and dotted lines in Fig. 6 show the contributions of each p- and d-band, respectively. Clearly low temperature dependence of $\lambda^2(0)/\lambda^2(T)$ is dominated by the d-band with the smallest T_c, whereas the high temperature behavior results from the p-band with the larger T_c. Notice that this analysis was applied for more reliable $\lambda(0)=143$ nm data. The reduced energy gap for p-band, $2\Delta_p(0)/k_BT_c^p=2.81$, is rather small relative to the BCS value 3.52, while d-band value, $2\Delta_d(0)/k_BT_c^d=6.44$, is twice as big. Thus we suggest that ZrB_{12} may have two superconducting bands with different T_c and order parameters. Notice that this unusual conclusion may be right for two bands in the limit of zero interband coupling in agreement with resistivity data. Also, the $\Delta(0)$ of ZrB_{12} may not be constant over the Fermi surface. Here we just tried to fit a data assuming two gap distinct values.

We based our conclusion on the two-gap model for dirty-limit superconductors, suggested by Gurevich.[45] In this model, we can write

$$\frac{1}{\lambda^2(0)}=\frac{4\pi^2e^2}{\hbar c^2}(N_p\Delta_pD_p+N_d\Delta_dD_d)=\frac{1}{\lambda_p^2(0)}+\frac{1}{\lambda_d^2(0)}, \quad (12)$$

where N_i, Δ_i, and D_i are the density of states, the energy gap, and the diffusivity in p- and d-bands, respectively.

The calculated band structure of ZrB_{12} is composed of three Fermi surface sheets: an open sheet along the ΓL direction with $k_{\Gamma X}=0.47$ Å^{-1}, a quasispherical sheet at point X ($k_{X\Gamma}=0.37$ Å^{-1}), and a small sheet at point K ($k_{K\Gamma}=0.14$ Å^{-1}).[20] It is not clear from Ref. 20 whether the wave functions of carriers on these sheets are due to predominantly p- or d-states. However, it follows that the dominant contribution to the density of states $N(E_F)$ is made by the Zr_{4d} and B_{2p} states, with $N_d=7.3\times10^{21}$ st/eV cm^3 and $N_p=8.7\times10^{21}$ st/eV cm^3, respectively.[20] The B_{2p} bonding states are responsible for the formation of B_{12} intracluster covalent bonds. In turn, Zr_{4d} bands are due to Zr sublattice. A much smaller boron isotope effect on T_c in comparison with Zr isotopic substitution[13,14] may be an indication of the existence of two separate subsystems with different gaps and T_c values. We use this two band approach [Eq. (12)] to obtain p-band diffusivity of $D_p=57$ cm^2/s and d-band diffusivity of $D_d=10$ cm^2/s. Note that there is almost a six times difference between the p- and d-band diffusivity. We use this result for our discussion of $H_{c2}(T)$ data in the following paragraph.

The important goal of this paper is comparison of ZrB_{12} and MgB_2 data. For comparison, in Fig. 4 we show the temperature variation of $\lambda(T)$ and in Fig. 6 a $\lambda^2(0)/\lambda^2(T)$ versus reduced temperature T/T_c for the best MgB_2 film as determined from the one-coil technique [Eq. (2)] and inversion procedure from Eq. (4) with $\lambda(0)=114$ nm. The solid line represents BCS single gap calculations by the aid of a single term of Eq. (11) and using finite energy gap [$\Delta(0)=1.93$ meV] as the fit parameter. According to Fig. 6, there is a very good agreement between experimental data and the single band BCS curve over the full temperature range. Simple conventional s-wave dirty case fit by Eq. (9) agrees remarkably well with the low-T data at $T<T_c/2$ too. The reduced energy gap $2\Delta(0)/k_BT_c$ is evaluated to be 1.2. It is actually within the range of values for 3D π bands obtained by PCS on MgB_2 single crystals [$\Delta(0)=2.9$ meV],[46] and it agrees with $\lambda(T)$ data obtained from similar radio-frequency experiments on single crystals (1.42 meV[47]), thin films (2.3 meV[33]), and with the theoretical prediction of the two-band model.[24] Rather small $2\Delta(0)/k_BT_c$ observed correspond to the smallest energy gap in the two-gap model for the 3D π band. Notice that we studied here the penetration depth in the ab plane due to the samples being c-axis oriented thin films. This feature predicts that our $\lambda_{ab}(T)$ is determined by the small energy gap for the π-band. Both $\lambda(0)$ and $\Delta(0)$ are consistent with microwave measurements on similar c-axis oriented thin films (107 nm and 3.2 meV, respectively).[48]

V. UPPER AND LOWER CRITICAL MAGNETIC FIELD

We now turn to the electronic transport data acquired in magnetic field. We measured the dependence of ρ on magnetic field H in the temperature range between 0.35 and 6 K in two different magnets at NHMFL, Tallahassee, FL as well as in our superconducting coil. The first magnet was resistive coil Bitter magnet, and second one was superconducting magnet. Figure 7 displays the resistive magnetic field transitions at various temperatures down to 0.35 K in the field oriented along the sample bar. Two features are clearly seen: (i) as temperature decreases the resistive transition continuously moves to higher fields without any saturation, and (ii) longitudinal magnetoresistivity in the normal state is very small. We used several different approaches to extract $H_{c2}(T)$ from our data. Initially, we extended the maximal derivative $d\rho/dH$ line (dashed line in Fig. 7) up to the normal state $\rho(T)$ level. The crossing point of this line and the normal state $\rho(T)$ gave us the estimate for H^*_{c2} at various temperatures, as is indicated by the arrow. Despite a clear broadening at the higher fields, the onset of the resistive transition remains well-defined even at rather low temperatures. To obtain an alternative estimate for H_{c2}, we fitted the field dependence of $\rho(H)$ by a cubic polynomial and calculated the derivative $d\rho/dH$. We defined H_{c2} as the field where $d\rho/dH$ just starts to deviate from zero (see Fig. 7). It is important to mention that even in single crystalline samples the resistance can be affected by the defects and surface superconductivity. To get even better fill for H_{c2} we used our $\lambda(H)$ data. Figure 8 shows a plot of the λ versus the longitudinal magnetic field H measured at various temperatures. [We use the same rectangular coil LC technique as for zero field $\lambda(T)$ measurements.] To avoid demagnetization effects like in Refs. 19 and 21–23 we oriented our bar-shape sample with its longer side parallel to the external dc field. Changes in the magnetic dependence of $\lambda(H)$ are directly proportional to the radio-frequency susceptibility of the sample and reflect the bulk properties of it. To deduce the H_{c2} from $\lambda(H)$, we used approaches similar to those applied to $\rho(T)$ data, i.e., a straight-line fit representing the maximum of derivative $d\lambda/dH$ (dashed line in Fig. 8) was extended up to the normal state. H^*_{c2} was defined as a crossing point of this line with normal state skin depth δ. Figure 8 clearly demonstrates a well-defined onset of $\lambda(H)$ transition. We used this onset to estimate H_{c2}.

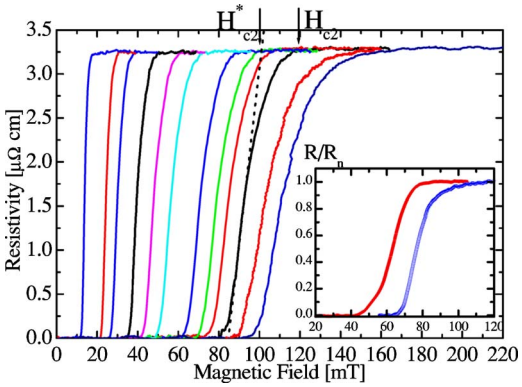

FIG. 7. (Color online) Resistivity of ZrB_{12} in the vicinity of the superconducting transition as a function of H at different T: 5.45, 5.08, 4.9, 4.26, 3.72, 3.26, 2.59, 2.16, 1.85, 1.39, 1.05, and 0.35 K from left to right. The dotted line and the arrows describe how the H_{c2} has been established. The inset shows the $R(H)/R_n$ near the transition at $T=2.3$ K for the same sample (right line) and a sample cut from the ZrB_2 rich part of an ingot (left curve).

Figure 9 shows the magnetic field $\lambda(H)$ behavior at very small fields. The $\lambda(H)-\lambda(0)$ curves display clear linear de-

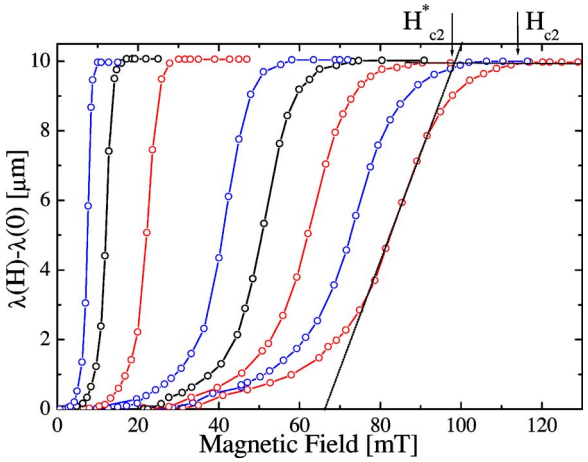

FIG. 8. (Color online) Magnetic field variation of $\lambda(H)$ of a single crystal ZrB_{12} sample at different temperatures: 5.66, 5.53, 5.02, 4.06, 3.45, 2.84, 2.15, and 1.43 K, from left to right. The solid lines are guides for the eye. The dotted line and the arrows describe how H_{c2}^{*} and H_{c2} have been deduced.

pendence at low fields caused by the Meissner effect. We determined the value of H_{c1} from the crossing point of two linear dependencies below and above the break point on $\lambda(H)$ (see Fig. 9).

Figure 10 presents the $H_{c2}^{*}(T)$ dependence obtained from extrapolation of the maximum of slopes of both $\rho(H)$ and $\lambda(H)$, as well as those defined at the onsets of the finite $\rho(H)$ and $\lambda(H)$. In the same figure we also plot the $H_{c1}(T)$, acquired by using the break point of $\lambda(H)$ criteria as the definition of the lower critical magnetic field. A remarkable feature of this plot is an identical linear increase of H_{c2} with decreasing temperature for each of the methods of defining H_{c2}. As we can see from this figure, the H_{c2} data obtained at three different magnets agree remarkably well and are aligned along corresponding straight lines indicating linear $H_{c2}(T)$ dependence down to 0.35 K.

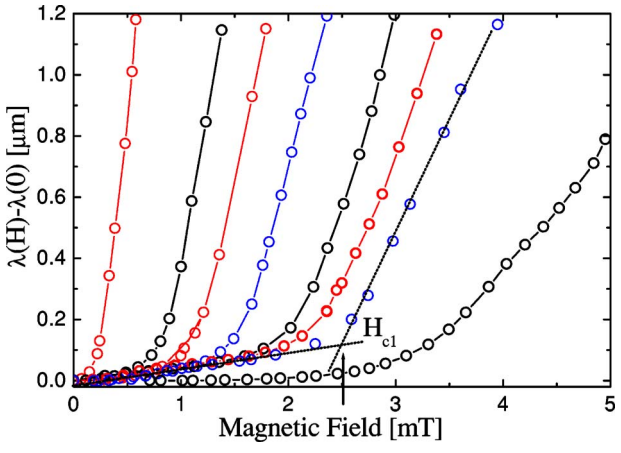

FIG. 9. (Color online) Low magnetic field variation of $\lambda(T)$ of a ZrB_{12} sample at small fields at various temperatures: 5.8, 5.2, 4.8, 4.4, 3.8, 3.5, 3.1, and 1.5 K, from left to right. The solid lines are guides for the eye. The dotted line is the linear extrapolation of the data used for H_{c1} determination.

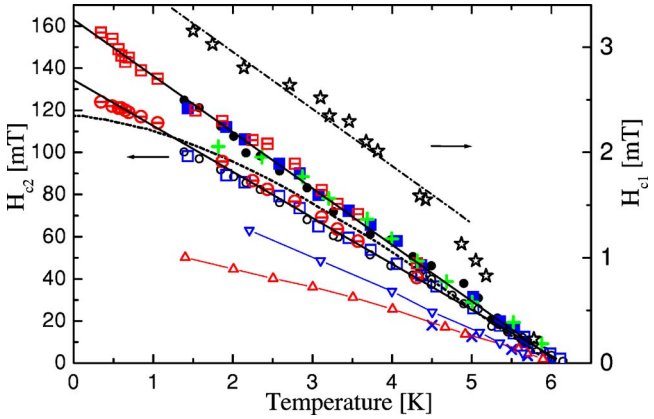

FIG. 10. (Color online) Temperature variations of $H_{c2}(T)$ and $H_{c1}(T)$ (stars) of ZrB_{12}. Symbols: $H_{c2}^{*}(T)$ determined from $\rho(H)$ (circles) and $\lambda(H)$ (squares) extrapolations; closed points are the onset $H_{c2}(T)$ data, as described in the text. Open circles and squares are $\rho(T)$ data obtained in NHMFL. Dotted line is the BCS $H_{c2}(T)$ data determined from the HW formula (Ref. 50). The straight crosses are PCS data (Ref. 21), tilted crosses are magnetization data (Ref. 22), up triangles are $C(H)$ data, and down triangles are the $\rho(H)$ data from Refs. 19 and 23.

To see whether one gap BCS model may work for ZrB_{12}, we extrapolate $H_{c2}(T)$ to zero temperature by use of the derivative of $dH_{c2}(T)/dT$ close to T_c and the assumption that the zero temperature $H_{c2}(0)=0.69T_c dH_{c2}/dT|_{T_c}$.[39] The resulting $H_{c2}(0)=114$ mT is substantially lower than the low temperature onset data below 3 K (see Fig. 10). Linear extrapolation of $H_{c2}(T)$ to $T=0$ gives $H_{c2}(0)=162$ mT. This value is almost the same as that obtained in the polycrystalline ZrB_{12} samples (150 mT).[16] We used this value to obtain the coherence length $\xi(0)$ by employing the relations $H_{c2}(0)=\phi_0/2\pi\xi^2(0)$. The latter yields $\xi(0)=45$ nm, which is substantially larger than a few angstroms coherence length of high-T_c superconductors.

In contrast to Refs. 19, 22, and 23 our estimations agree well with the Ginzburg-Landau parameter $\kappa=\lambda/\xi$. Using our values of λ_p and λ_d data we obtain $\kappa_p=3.8$ and $\kappa_d=5.8$. Both values of κ are larger then $1/\sqrt{2}$ that implies that ZrB_{12} is clearly a type II superconductor at all T. Using the GL expression for $H_{c1}(T)=\phi_0 \ln\kappa/4\pi\lambda^2$ we obtain $H_{c2}/H_{c1}=2\kappa^2/\ln\kappa$. From the value $H_{c2}(0)$ obtained above and the H_{c1} data from Fig. 9, we find $\kappa=6.3$ and $\lambda(0)=280$ nm which is in good agreement with the value $\lambda(0)=260$ nm obtained from the two gap BCS fit for d-band. One could argue that the $H_{c1}(T)$ obtained from our magnetic field measurements of $\lambda(H)$ may reflect the flux entry field because of the Bean-Livingston surface barrier, rather then true H_{c1}. However, the entry field $H_{BL}=H_{c1}\kappa/\ln\kappa$ (Ref. 49) is three times larger than H_{c1} even when one uses $\kappa=6.3$, so if we assume $\kappa=23$ given by a ratio of H_{c2}/H_{c1} we obtain zero temperature $\lambda(0)=1030$ nm, which is unreasonably large compared to one obtained from a BCS fit. This result is another confirmation of our suggestions.

In contrast to the conventional BCS theory,[50] $H_{c2}(T)$ dependence is linear over an extended temperature range with no evidence of saturation down to 0.35 K. Similar linear

$H_{c2}(T)$ dependence has been observed in MgB_2 (Refs. 51 and 52) and $BaNbO_x$ (Ref. 53) compounds. One can describe this behavior of upper critical field using the two gap approach. According to Gurevich,[45] the zero-temperature value of the $H_{c2}(0)$ is significantly enhanced in the two gap dirty limit superconductor model:

$$H_{c2}(0) = \frac{\phi_0 k_B T_c}{1.12\hbar\sqrt{D_1 D_2}} \exp\left(\frac{g}{2}\right), \tag{13}$$

as compared to the one-gap dirty limit approximation $H_{c2}(0) = \phi_0 k_B T_c / 1.12\hbar D$. Here g is a rather complicated function of the matrix of the BCS superconducting coupling constants.

In the limit of $D_2 \ll D_1$ we can simply approximate $g \approx |\ln(D_2/D_1)|$. The large ratio of D_2/D_1 leads to the enhancement of $H_{c2}(0)$ and results in the upward curvature of the $H_{c2}(T)$ close to $T=0$.[45] According to our $\lambda(T)$ data (see above), we found very different diffusivities for p- and d-bands: $D_p/D_d \approx 3$. Thus we can speculate that the limiting value of $H_{c2}(0)$ is dominated by d-band with lower diffusivity $D_d = 17$ cm^2/s, while the derivative dH_{c2}/dT close to T_c is due to larger diffusivity band ($D_p = 56$ cm^2/s). Indeed, simple estimation of $D_p = 4\phi_0 k_B/\pi^2\hbar(dH_{c2}/dT) = 40$ cm^2/s from a derivative $dH_{c2}/dT = 0.027T/\mathrm{K}$ close to T_c gives almost the same diffusivity relative to one estimated from $\lambda(T)$ for the p-band. Thus we believe that the two gap theoretical model of Gurevich qualitatively explains the unconventional linear $H_{c2}(T)$ dependence, which supports our conclusion about the two gap nature of superconductivity in ZrB_{12}.

The possibility of the multigap nature of the superconducting state was predicted for a multiband superconductor with large difference of the e-p interaction at different FS sheets (see Ref. 24 and references therein). To date MgB_2 has been the only compound with the behavior consistent with the idea of two distinct gaps with the same T_c. We believe that our data can add ZrB_{12} as another unconventional example of multigap and multi-T_c superconductor. This conclusion contradicts several existing publications, however, we believe we can successfully defend our idea.

The $H_{c2}(T)$ dependence of ZrB_{12} single crystals from the same Kiev group has been measured by three different groups mentioned above and are plotted in Fig. 10. Clearly, our $H_{c2}(T)$ data are very similar to those obtained by Daghero *et al.*[21] (straight crosses). The agreement is nearly perfect except the last data point at 1.8 K. The disagreement is in the interpretation. The authors of Ref. 21 concluded that ZrB_{12} is a conventional one gap s-wave superconductor with $\Delta(0) = 1.22$ meV. Thus a strong coupling scenario with reduced energy gap of $2\Delta(0)/k_B T_c = 4.8$ was proposed. One should note, however, that the gap signature in PCS data has been observed in a temperature range close to T_c(4.2–6 K), although the second gap signature feature should have been seen below $T_c^d = 4.35$ K, and could have been simply missed by the authors of Ref. 21 because of the limited temperature range of their measurements.

There is nearly a two times difference between $H_{c2}(T)$ obtained from tunneling and magnetic characterization data of Tsindlekht *et al.*[22] The same can be said about $H_{c2}(T)$ obtained from $C(H)$ and $\rho(H)$ data of Lortz *et al.*[19] and Wang *et al.*[23] Tsindlekht *et al.* concluded that ZrB_{12} is a type-II superconductor with the Ginzburg-Landau parameter κ slightly above the marginal value of $1/\sqrt{2}$. At the same time Wang *et al.*[23] observed a crossover between type-I and type-II behavior of $C(H)$ at 4.7 K in contrast to our data. In all those approximations, the validity of the one gap BCS picture is implicitly assumed. Large contradiction between the $\rho(H)$ and $C(H)$ data (see Fig. 10) was attributed to surface superconductivity. One can mention another possible reason for this contradiction. In particular, data of Ref. 23 have been measured on the samples cut by a diamond saw without chemical etching of the surface damaged layer. This procedure may create a strong concentration gradient of boron in a surface layer and a substantial manifestation of the surface barriers for the flux lines resulting in this contradiction. One can also note that the discrepancies in $H_{c2}(T)$ can be due to potentially large nonhomogeneity of the ZrB_{12} samples. Indeed, the Fig. 7 inset clearly demonstrates different transitions for our sample with no inclusions of ZrB_2 and the sample cut from ZrB_2 reaches part of an ingot (left line).

We believe that this inconsistency of our data and the data of Refs. 19 and 21–23 can be (i) due to the two gap nature of superconductivity in ZrB_{12}, (ii) due to large uncertainty in determining of the zero temperature gap from very narrow temperature range of the measurements, and (iii) last but not least due to potentially large nonhomogeneity of the ZrB_{12} samples that could have been used by those authors (see Fig. 2). Although observed two gap behavior of $\lambda^2(0)/\lambda^2(T)$ in ZrB_{12} is similar to that in high-T_c superconductors, observation of two different T_c in these bands is unconventional. This also relates to the linear $H_{c2}(T)$ dependence in the wide temperature range up to T_c. Striking two-gap BCS behavior observed calls certainly for a new study of low-T energy gap and $H_c(T)$ of ZrB_{12} for understanding the nature of superconductivity in this cluster compound.

VI. CONCLUSIONS

We performed systematic study of the temperature and magnetic field dependencies of the resistivity, magnetic penetration depth, lower, $H_{c1}(T)$, and upper, $H_{c2}(T)$, critical magnetic fields of the single crystals dodecaboride ZrB_{12} and resistivity of diboride ZrB_2, as well as the magnetic penetration depth in thin films of MgB_2. While the temperature dependence of $\lambda(T)$ in thin film MgB_2 is well described by an isotropic single gap s-type order parameter, we find unconventional behavior of ZrB_{12} superfluid density with pronounced shoulder at T/T_c equal to 0.65. The $H_{c2}(T)$ dependencies have been deduced from the $\rho(H)$ and $\lambda(H)$ data. Both techniques reveal an unconventional linear temperature dependence of $H_{c2}(T)$, with a considerably low value of $H_{c2}(0) = 0.16$ T. We conclude therefore that ZrB_{12} presents a evidence of the unconventional two-gap superconductivity with different Δ and T_c in the different bands.

ACKNOWLEDGMENTS

We would like to thank V. F. Gantmakher, A. Gurevich, R. Huguenin, D. van der Marel, and I. R. Shein for very useful

discussions, V. B. Filipov, A. B. Lyashenko, and Yu. B. Paderno for preparation of ZrB_{12} and ZrB_2 single crystals, Hong-Ying Zhai, H. M. Christen, M. P. Paranthaman, and D. H. Lowndes for providing us high-quality MgB_2 films, A. Suslov for help in low-T measurements in NHMFL, L. S. Uspenskaja for help in metallographic analysis, and L. V. Gasparov for very useful cooperation in paper preparation. This work was supported by the Russian Council on High-Temperature Superconductivity (Grant Volna 4G), the Russian Scientific Programs: Surface Atomic Structures (Grant No. 4.10.99) and Synthesis of Fullerens and Other Atomic Clusters (Grant No. 541-028), Russian Ministry of Industry, Science and Technology (Grant Msh-2169.2003.2), the Russian Foundation for Basic Research (Grant No. 02-02-16874-a), and by the INTAS (Grant No. 2001-0617). A portion of this work was performed at the National High Magnetic Field Laboratory, which is supported by NSF Cooperative Agreement No. DMR-0084173 and the State of Florida.

[1] J. Nagamatsu, N. Nakagawa, T. Muranaka, Y. Zanitani, and J. Akimitsu, Nature (London) **410**, 63 (2001).
[2] V. A. Gasparov, N. S. Sidorov, I. I. Zver'kova, and M. P. Kulakov, JETP Lett. **73**, 601 (2001).
[3] Z. Fisk, in *Boron-Rich Solids*, edited by D. Emin, T. L. Asclage, A. C. Switendick, B. Morosin, and C. L. Beckel, AIP Conf. Proc. No. 231 (AIP, New York, 1991), p. 155.
[4] A. Yamamoto, C. Takao, T. Masui, M. Izumi, and S. Tajima, Physica C **383**, 197 (2002).
[5] R. Escamilla, O. Lovera, T. Akachi, A. Durán, R. Falconi, F. Morales, and R. Escudero, J. Phys.: Condens. Matter **16**, 5979 (2004).
[6] D. P. Young, R. G. Goodrich, P. W. Adams, J. Y. Chan, F. R. Fronczek, F. Drymiotis, and L. L. Henry, Phys. Rev. B **65**, 180518(R) (2002).
[7] N. Ashcroft, Phys. Rev. Lett. **21**, 1748 (1968).
[8] J. Kortus, I. I. Mazin, K. D. Belashchenko, V. P. Antropov, and L. L. Boyer, Phys. Rev. Lett. **86**, 4656 (2001).
[9] K. Tanigaki, T. W. Ebbesen, S. Saito, J. Mizuki, J. S. Tsai, Y. Kubo, and S. Kuroshima, Nature (London) **352**, 222 (1991).
[10] O. Gunnarsson, Rev. Mod. Phys. **69**, 575 (1997).
[11] B. T. Matthias, T. H. Geballe, K. Andres, E. Corenzwit, G. Hull, and J. P. Maita, Science **159**, 530 (1968).
[12] Y. Paderno, N. Shitsevalova, I. Batko, K. Flahbart, H. Misiorek, J. Mucha, and A. Jezowski, J. Alloys Compd. **219**, 215 (1995).
[13] C. W. Chu and H. H. Hill, Science **159**, 1227 (1968).
[14] Z. Fisk, A. C. Lawson, B. T. Matthias, and E. Corenzwit, Phys. Lett. A **37**, 251 (1971).
[15] V. A. Gasparov, N. S. Sidorov, M. P. Kulakov, I. I. Zver'kova, V. P. Kobyakov, Hong-Ying Zhai, H. M. Christen, M. P. Paranthaman, and D. H. Lowndes, *Book of abstracts of BOROMAG Conf. (Genoa, Italy)* (2002), p. 52.
[16] V. A. Gasparov, N. S. Sidorov, I. I. Zver'kova, S. S. Khassanov, and M. P. Kulakov, JETP **128**, 115 (2005).
[17] V. A. Gasparov, N. S. Sidorov, I. I. Zver'kova, V. B. Filipov, A. B. Lyashenko, and Yu. B. Paderno, *Book of Abstracts of 6th Biennial International Workshop on Fullerenes and Atomic Clusters* (St. Petersburg, 2003), p. 83; *Book of Abstracts of 10th International Workshop on Oxide Electronics* (Augsburg, 2003), p. 184.
[18] V. A. Gasparov, M. P. Kulakov, N. S. Sidorov, I. I. Zver'kova, V. B. Filipov, A. B. Lyashenko, and Yu. B. Paderno, Pis'ma Zh. Eksp. Teor. Fiz. **80**, 376 (2004) [JETP Lett. **80**, 330 (2004)].
[19] R. Lortz, Y. Wang, S. Abe, C. Meingast, Yu. B. Paderno, V. Filippov, and A. Junod, Phys. Rev. B **72**, 024547 (2005).
[20] I. R. Shein and A. L. Ivanovskii, Fiz. Tverd. Tela (Leningrad) **45**, 1363 (2003) [Phys. Solid State **45**, 1429 (2003)].
[21] D. Daghero, R. S. Gonnelli, G. A. Ummarino, A. Calzolari, V. Dellarocca, V. A. Stepanov, V. B. Filippov, and Y. B. Paderno, Supercond. Sci. Technol. **17**, S250 (2004).
[22] M. I. Tsindlekht, G. I. Leviev, I. Asulin, A. Sharoni, O. Millo, I. Felner, Yu. B. Paderno, V. B. Filippov, and M. A. Belogolovskii, Phys. Rev. B **69**, 212508 (2004); G. I. Leviev, V. M. Genkin, M. I. Tsindlekht, I. Felner, Yu. B. Paderno, and V. B. Filippov, cond-mat/0410356 (unpublished).
[23] Y. Wang, R. Lortz, Yu. Paderno, V. Filippov, S. Abe, U. Tutsch, and A. Junod, Phys. Rev. B **72**, 024548 (2005).
[24] A. Brinkman, A. A. Golubov, H. Rogalla, O. V. Dolgov, J. Kortus, Y. Kong, O. Jepsen, and O. K. Andersen, Phys. Rev. B **65**, 180517(R) (2001); A. A. Golubov, A. Brinkman, O. V. Dolgov, J. Kortus, and O. Jepsen, *ibid.* **66**, 054524 (2002).
[25] Yu. Paderno, A. Liashchenko, V. Filipov, and A. Dukhnenko, *Science for Materials in the Frontier of Centuries: Advantages and Challenges*, edited by V. V. Skorokhod (IPM NASU, Kiev, 2002), p. 347.
[26] A. Leithe-Jasper, A. Sato, and T. Tanaka, Z. Kristallogr. - New Cryst. Struct. **217**, 319 (2002).
[27] M. Paranthaman, C. Cantoni, H. Y. Zhai, H. M. Christen, T. Aytug, S. Sathyamurthy, E. D. Specht, J. R. Thompson, D. H. Lowndes, H. R. Kerchner, and D. K. Christen, Appl. Phys. Lett. **78**, 3669 (2001).
[28] V. A. Gasparov, M. R. Mkrtchyan, M. A. Obolensky, and A. V. Bondarenko, Physica C **1**, 197 (1994).
[29] C. Varmazis and M. Strongin, Phys. Rev. B **10**, 1885 (1974).
[30] V. A. Gasparov and A. P. Oganesyan, Physica C **178**, 445 (1991).
[31] A. Gauzzi, J. Le Cochec, G. Lamura, B. J. Jönsson, V. A. Gasparov, F. R. Ladan, B. Plaçais, P. A. Probst, D. Pavuna, and J. Bok, Rev. Sci. Instrum. **71**, 2147 (2000).
[32] V. A. Gasparov, G. Tsydynzhapov, I. E. Batov, and Qi Li, J. Low Temp. Phys. **139**, 49 (2005).
[33] G. Lamura, E. Di Gennaro, M. Salluzzo, A. Andreone, J. Le Cochec, A. Gauzzi, C. Cantoni, M. Paranthaman, D. K. Christen, H. M. Christen, G. Giunchi, and S. Ceresara, Phys. Rev. B **65**, 020506(R) (2001).
[34] I. R. Shein, N. I. Medvedeva, and A. L. Ivanovskii, Fiz. Tverd. Tela (Leningrad) **45**, 1541 (2003) [Phys. Solid State **45**, 1617 (2003)].
[35] J. M. Ziman, *Electrons and Phonons, Theory of Transport Phenomena in Solids* (Oxford University Press, Oxford, England, 1960).
[36] V. F. Gantmakher, Rep. Prog. Phys. **37**, 317 (1974).
[37] V. A. Gasparov and R. Huguenin, Adv. Phys. **42**, 393 (1993).

[38] J. Halbritter, Z. Phys. **243**, 201 (1971).
[39] J. B. Ketterson and S. N. Song, *Superconductivity* (Cambridge University Press, Cambridge, England, 1999).
[40] W. N. Hardy, D. A. Bonn, D. C. Morgan, R. Liang, and K. Zhang, Phys. Rev. Lett. **70**, 3999 (1993).
[41] D. A. Bonn, S. Kamal, K. Zhang, R. Liang, D. J. Baar, E. Klein, and W. N. Hardy, Phys. Rev. B **50**, 4051 (1994).
[42] N. Klein, N. Tellmann, H. Schulz, K. Urban, S. A. Wolf, and V. Z. Kresin, Phys. Rev. Lett. **71**, 3355 (1993).
[43] N. Schopohl and O. V. Dolgov, Phys. Rev. Lett. **80**, 4761 (1998); **81**, 4025 (1998).
[44] A. Carrington, F. Manzano, R. Prozorov, R. W. Giannetta, N. Kameda, and T. Tamegai, Phys. Rev. Lett. **86**, 1074 (2001).
[45] A. Gurevich, Phys. Rev. B **67**, 184515 (2003).
[46] R. S. Gonnelli, D. Daghero, G. A. Ummarino, V. A. Stepanov, J. Jun, S. M. Kazakov, and J. Karpinski, Phys. Rev. Lett. **89**, 247004 (2002).
[47] F. Manzano, A. Carrington, N. E. Hussey, S. Lee, A. Yamamoto, and S. Tajima, Phys. Rev. Lett. **88**, 047002 (2002).
[48] B. B. Jin, N. Klein, W. N. Kang, H.-J. Kim, E.-M. Choi, S.-I. Lee, T. Dahm, and K. Maki, Phys. Rev. B **66**, 104521 (2002).
[49] P. G. de Gennes, *Superconductivity of Metals and Alloys* (Addison-Wesley, New York, 1989), p. 79.
[50] E. Helfand and N. R. Werthamer, Phys. Rev. Lett. **13**, 686 (1964); Phys. Rev. **147**, 288 (1966).
[51] L. Lyard, P. Samuely, P. Szabo, T. Klein, C. Marcenat, L. Paulius, K. H. P. Kim, C. U. Jung, H.-S. Lee, B. Kang, S. Choi, S.-I. Lee, J. Marcus, S. Blanchard, A. G. M. Jansen, U. Welp, G. Karapetrov, and W. K. Kwok, Phys. Rev. B **66**, 180502(R) (2002).
[52] A. V. Sologubenko, J. Jun, S. M. Kazakov, J. Karpinski, and H. R. Ott, Phys. Rev. B **65**, 180505(R) (2002).
[53] V. A. Gasparov, S. N. Ermolov, G. K. Strukova, N. S. Sidorov, S. S. Khassanov, H.-S. Wang, M. Schneider, E. Glaser, and W. Richter, Phys. Rev. B **63**, 174512 (2001); V. A. Gasparov, S. N. Ermolov, S. S. Khasanov, G. K. Strukova, L. V. Gasparov, H.-S. Wang, Qi Li, M. Schnider, W. Richter, E. Glaser, F. Schmidl, P. Seidel, and B. L. Brandt, Physica B **284–288**, 1119 (2000).